Supporting Information

Beerling et al. 10.1073/pnas.1102409108

SI Methods

Modeling Ancient "Greenhouse" Climates. HadCM3L is a coupled ocean-atmosphere model needing no flux correction terms that is well-documented and tested elsewhere (1, 2). This particular version uses the standard resolution atmosphere (3.75° × 2.5°× 19 levels) coupled to an equivalent resolution ocean (3.75°× 2.5° × 20 levels), with MOSES 2.2 land surface scheme (3), and a radiation scheme explicitly representing the relevant trace GHGs (4).

We modified HadCM3L with early Eocene and late-Cretaceous palaeogeographies provided by Paul Markwick (5). The solar constant was modified to be appropriate for the relevant period; specifically 0.4% reduction for early Eocene and 0.76% reduction for late Cretaceous. In the standard HadCM3 model, ozone concentrations vary with latitude and height and month, but are otherwise constant. The climate model was modified so that ozone was predicted to vary according to the tropopause height, with a low value in the troposphere (from STOCHEM), intermediate value at the tropopause, and high value in stratosphere.

For each time period and suite of greenhouse gases (GHGs), the baseline simulations were spun-up for at least 1,500 model years to ensure the equilibrium in the ocean-atmosphere system. Subsequent sensitivity experiments were run for 150–200 years, a sufficient duration to reach near equilibrium in the surface conditions.

Modeling Terrestrial Vegetation Biogeography, Structure, and Function. The Sheffield Dynamic Global Vegetation Model (SDGVM) simulates global patterns of net primary production (NPP), leaf area index (LAI), and the distribution of plant functional types (PFTs) from monthly inputs of temperature, precipitation, relative humidity, and global datasets of soil texture (6, 7). Core modules of net photosynthesis, stomatal conductance, canopy transpiration, uptake of mineralized nitrogen, and responses of these attributes to changes in soil water supply are detailed, and rigorously evaluated against field observations (6–8). A key feature of SDGVM is the coupling of above- and below-ground C and N cycles. Litter production influences soil C and N pools via the Century soil nutrient cycling model (9), which feedback to influence above-ground primary productivity. SDGVM includes a fire submodule. It uses the availability of litter, and the calculated water content of the litter layer, to estimate the fire return interval. A random number generator determines whether an area is burned or not, if the litter water content reaches critical dryness (10). When a fire occurs, 80% of the above-ground carbon and nitrogen is lost during combustion. Monthly estimates of carbon released by burning provide a means of scaling the associated release of reactive trace gases (CH_4, NO_x, N_2O and CO) (11).

Local and global-scale SDGVM predictions of NPP, LAI, and PFT distributions have been extensively and successfully evaluated against a wide range of measurements, field observations and satellite products (7). Global NPP for the contemporary climate and CO_2 (62 $Gt\,C\,yr^{-1}$) agrees with the satellite-based estimated range (55–60 $Gt\,C\,yr^{-1}$) (12). Sensitivity of SDGVM NPP predictions to CO_2 and climate are similar to those of other Dynamic Global Vegetation Models (13, 14). The CO_2 fertilization response of NPP compares favorably to that reported in Free Air Carbon Dioxide Enrichment experiments for temperate forested sites in North America and Italy (15).

Global simulations of the geographical distribution of PFTs depend on NPP, LAI, relative growth rates, and minimum temperature thresholds. In the Eocene, these are similar to that produced independently by others (16) (Fig. S2), and to that reconstructed from paleobotancial information (17). Late-Cretaceous simulated global distribution of PFTs (Fig. S2) is broadly comparable with a global vegetation reconstruction from fossil plants and other geologic evidence (7, 18). Wetland areas and trace gas fluxes are given in Table S1.

Reactive Trace Gas Fluxes. Monthly wetland CH_4 emissions are computed with a process-based model (19) coupled to the carbon cycle and land surface hydrology calculated by SDGVM with monthly climate fields from HadCM3L. The coupled CH_4 emissions model describes the dependence of anaerobic microbial CH_4 production and aerobic oxidation on temperature, vegetation activity (gross primary productivity), soil respiration and soil water table depth (19). Wetland CH_4 emissions were modified to include the effects of orography by scaling with a linear function of subgrid orographic variance (20). Emissions of CH_4 from termites and oceans are assumed to be the same as in the preindustrial, but with altered distributions according to the land and sea areas (Table S1). These procedures likely mean the contribution of biogenic CH_4 fluxes from these sources are conservative.

Monthly soil biogenic NO_x fluxes are calculated with an empirical model describing their dependence on temperature, precipitation and canopy deposition (21). Lightning NO_x emissions were calculated with the interactive NO_x lightning scheme in STOCHEM (22, 23) using total number of lightning flashes from cloud top height and different formulae for continental and maritime clouds. Monthly soil biogenic N_2O fluxes are calculated with an empirical model as a function of monthly values of soil moisture and temperature, soil N status and NPP (24).

Monthly emissions of volatile organic compounds (VOCs) from terrestrial vegetation are predicted using a global scheme describing their dependence on temperature, photosynthetically active radiation, vegetation type, and canopy biomass (25). We account for SDGVM-derived land surface vegetation biogeography and monthly LAIs (20). Biogenic emissions of CH_4, N_2O, isoprene, soil NO_x, lightning NO_x, and fluxes of reactive trace gases emitted from biomass burning are verified by observations or within previous estimates from modeling studies (20).

Atmospheric Chemistry Calculations. Trace gas emissions, calculated globally on a monthly basis, provide inputs to the updated version of the Lagrangian chemistry model STOCHEM (22) on an emissions grid of 5° × 5°, and 9 equally spaced levels. STOCHEM includes 71 species that captures a reasonable representation of tropospheric chemistry (22, 26, 27) but does not include the full range of stratospheric ozone reactions. STOCHEM includes a method that uses a simple relaxation scheme for stratospheric ozone. The effects of warmer tropospheric temperatures (caused by $2 \times CO_2$ and $4 \times CO_2$ concentrations) on stratospheric ozone are not included in our simulations. These effects are complex, reflecting the balance between transport and chemical processes; for example, Rind et al. (28), in a $2 \times CO_2$ simulation, found that ozone increased in the upper stratosphere and decreased in the lower stratosphere leading to no large net change in column ozone. Changes in the distribution/magnitude of stratospheric ozone will also change tropospheric photolysis rates. However, recent studies with a version of STOCHEM coupled to a full stratospheric chemistry scheme (29) indicate that the effects on tropospheric ozone are typically dominated by changes in STE rather than changes in photolysis rates.

In intermodel comparisons, STOCHEM compares favorably with other chemistry schemes in terms of its predicted changes in tropospheric ozone concentrations (30, 31), indicating its utility for the present study. We coupled STOCHEM to HadCM3L at 3 hourly intervals and integrated all simulations until an equilibrium atmosphere was achieved, typically within 30–40 years. Full tropospheric methane, hydroxyl radical and ozone budgets, burdens, and lifetimes for the simulations are reported in Tables S2–S4.

Sources of Paleoclimate Data in Fig. 4. Eocene proxy terrestrial data from refs. 32–34, and sea-surface temperature data from refs. 35–38. Late-Cretaceous proxy terrestrial data from refs. 39–41, sea-surface temperature data from refs. 42–48.

1. Pope VD, et al. (2000) The impact of new physical parametrizations in the Hadley Centre climate model: HadAM3. *Clim Dynam* 16:123–146.
2. Gordon C, et al. (2000) The simulation of SST, sea ice extents and ocean heat transports in a version of the Hadley Centre coupled model without flux adjustments. *Clim Dynam* 16:147–168.
3. Essery RL, Best M, Cox PM (2001) *MOSES 2.2 Technical Documentation* Hadley Centre Technical Note 30 (Met Office, London).
4. Edwards JM, Slingo A (1996) Studies with a flexible new radiation code 1. Choosing a configuration for a large-scale model. *Q J Roy Meteor Soc* 122:689–719.
5. Markwick PJ, Valdes PJ (2004) Palaeo-digital elevation models for use as boundary conditions in coupled ocean-atmosphere GCM experiments: A Maastrichtian (late Cretaceous) example. *Palaeogeog Palaeoclim Palaeoecol* 213:37–63.
6. Woodward FI, Smith TM, Emanuel WR (1995) A global land primary productivity and phytogeography model. *Global Biogeochem Cy* 9:471–490.
7. Beerling DJ, Woodward FI (2001) *Vegetation and the Terrestrial Carbon cycle. Modelling the First 400 Million Years* (Cambridge University Press, Cambridge).
8. Beerling DJ, et al. (1997) Testing the responses of a dynamic global vegetation model to environmental change: A comparison of observations and predictions. *Global Ecol Biogeogr Lett* 6:439–450.
9. Parton WJ, et al. (1993) Observations and modeling of biomass and soil organic carbon matter dynamics for the grassland biomass worldwide. *Global Biogeochem Cy* 7:785–809.
10. Woodward FI, Lomas MR, Lee SE (2001) *Terrestrial Global Productivity* eds Roy J, Saugier B, Mooney HA (Academic Press, San Diego), pp 521–557.
11. Andreae MO, Merlet P (2001) Emissions of trace gases and aerosols from biomass burning. *Global Biogeochem Cy* 15:955–966.
12. Running SW, et al. (2004) A continuous satellite-derived measure of global terrestrial primary production. *Bioscience* 54:547–560.
13. Sitch S, et al. (2008) Evaluation of the terrestrial carbon cycle, future plant geography and climate-carbon cycle feedbacks using five dynamic global vegetation models (SDGVMs). *Global Change Biol* 14:2015–2039.
14. Hickler T, et al. (2008) CO_2 fertilization in temperate FACE experiments not representative of boreal and tropical forests. *Global Change Biol* 14:1–12.
15. Woodward FI, Kelly C (2008) Responses of global plant diversity capacity to changes in carbon dioxide concentration and climate. *Ecol Lett* 11:1229–1237.
16. Sewall JO, et al. (2000) Climate sensitivity to changes in land surface characteristics. *Glob Planet Change* 26:445–465.
17. Shellito CJ, Sloan LC (2006) Reconstructing a lost Eocene paradise: Part I. Simulating the change in global floral distribution at the initial Eocene thermal maximum. *Glob Planet Change* 50:1–17.
18. Upchurch GR, et al. (1998) Vegetation-climate-atmosphere interactions and their role in global warming during the latest Cretaceous. *Philos T R Soc S-A* 353:97–112.
19. Cao MK, Marshall S, Gregson K (1996) Global carbon exchange and methane emissions from natural wetlands: Application of a process-based model *J Geophys Res* 101:14399–14414.
20. Valdes PJ, Beerling DJ, Johnson CE (2005) The ice age methane budget. *Geophys Res Lett* 32:L02704, 10.1029/2004GL021004.
21. Yienger JJ, Levy H (1995) Empirical-model of global soil-biogenic NO_x emissions. *J Geophys Res* 100:11447–11464.
22. Stevenson D, et al. (2005) Impacts of climate change and variability on tropospheric ozone and its precursors. *Faraday Discuss* 130:41–57.
23. Price C, Penner J, Prather M (1997) NO_x from lightning. 1. Global distribution based on lightning physics. *J Geophys Res* 102:5929–5941.
24. Bouwman A, et al. (1993) Global analysis of the potential for N_2O production in natural soils. *Global Biogeochem Cy* 7:557–597.
25. Guenther A, et al. (1995) A global-model of natural volatile organic-compound emissions. *J Geophys Res* 100:8873–8892.
26. Collins WJ, Stevenson DS, Johnson CE, Derwent RG (1997) Tropospheric ozone in a global-scale three-dimensional Lagrangian model and its response to NO_x emission controls. *J Atmos Chem* 26:223–274.
27. Collins WJ, Stevenson DS, Johnson CE, Derwent RG (1999) Role of convection in determining the budget of odd hydrogen in the upper troposphere. *J Geophys Res* 104:26927–26941.
28. Rind D, et al. (2002) Sensitivity of tracer transports and stratospheric ozone to sea-surface temperature patterns in the doubled CO_2 climate. *J Geophys Res*, 10.1029/2006JG004800.
29. Tian W, et al. (2010) Effects of stratosphere-troposphere coupling on tropospheric ozone. *J Geophys Res* 115:D00M04, 10.1029/2009JD013515.
30. Gauss M, et al. (2006) Radiative forcing since preindustrial times due to ozone changes in the troposphere and the lower stratosphere. *Atmos Chem Phys* 6:575–599.
31. Stevenson DS, et al. (2006) Multimodel ensemble simulations of present-day and near-future tropospheric ozone. *J Geophys Res* 111:D08301, 10.1029/2005JD006338.
32. Greenwood DR, Wing SL (1995) Eocene continental climates and latitudinal temperature gradients. *Geology* 23:1044–1048.
33. Wilf P, et al. (2003) High plant diversity in Eocene South America: evidence from Patagonia. *Science* 300:122–125.
34. Francis JE, Poole I (2002) Cretaceous and early Tertiary climates of Antarctica: evidence from fossil wood. *Palaeogeogr Palaeoclim Palaeoecol* 182:47–64.
35. Pearson PN, et al. (2001) Warm tropical sea-surface temperatures in the late Cretaceous and Eocene epochs. *Nature* 413:481–487.
36. Sluijs A, et al. (2006) Subtropical Arctic Ocean temperatures during the Palaeocene/Eocene thermal maximum. *Nature* 441:610–613.
37. Hollis CJ, et al. (2009) Tropical sea temperatures in the high-latitude South Pacific during the Eocene. *Geology* 37:99–102.
38. Bijl PK, et al. (2009) Early Palaeogene temperature evolution of the southwest Pacific Ocean. *Nature* 461:776–779.
39. Tarduno JA, et al. (1998) Evidence for extreme climatic warmth from late Cretaceous Arctic vertebrates. *Science* 282:2241–2244.
40. Spicer RA, et al. (2008) The late Cretaceous continental interior of Siberia: a challenge for climate models. *Earth Planet Sc Lett* 267:228–235.
41. Miller IM, Brandon MT, Hickey LJ (2008) Using leaf margin analysis to estimate the mid-Cretaceous (Albian) paleolatitude of the Baja BC block. *Earth Planet Sc Lett* 245:95–114.
42. Spicer RA, Corfield RM (1992) A review of terrestrial and marine climates in the Cretaceous with implications for modelling the "Greenhouse Earth." *Geol Mag* 129:169–180.
43. Huber BT, Norris RD, MacLeod KG (2002) Deep-sea paleotemperature record of extreme warmth during the Cretaceous. *Geology* 30:123–126.
44. Jenkyns HC, et al. (2004) High temperatures in the late Cretaceous Arctic Ocean. *Nature* 432:888–892.
45. Steuber T, et al. (2005) Low-latitude seasonality of Cretaceous temperatures in warm and cold episodes. *Nature* 437:1341–1344.
46. Norris RD, Bice KL, Magno EA, Wilson PA (2002) Jiggling the tropical thermostat in the Cretaceous hothouse. *Geology* 30:299–302.
47. Schouten S, et al. (2003) Extremely high sea-surface temperatures at low latitudes during the middle Cretaceous as revealed by archeal membrane lipids. *Geology* 31:1069–1072.
48. Forster A, et al. (2007) Mid-Cretaceous (Albian–Santonian) sea-surface temperature record of the tropical Atlantic Ocean. *Geology* 35:919–922.

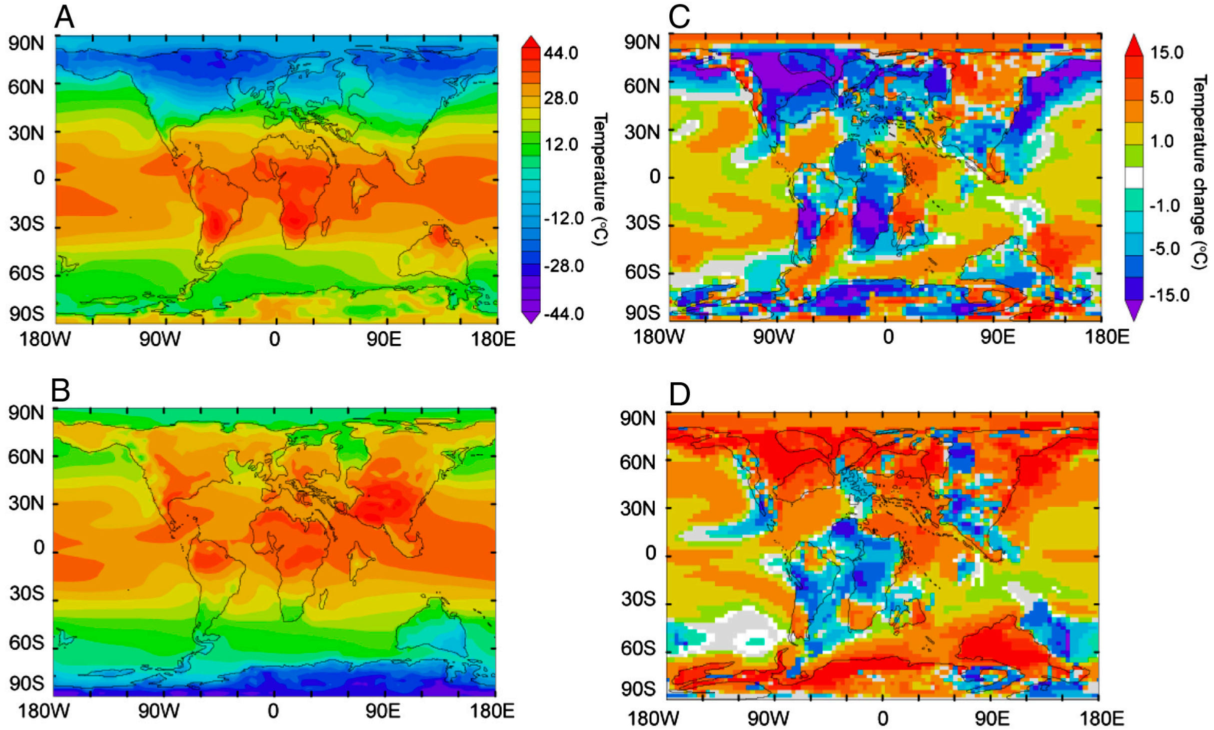

Fig. S1. Simulated Eocene $4 \times CO_2$ baseline surface temperatures during the northern hemisphere (*A*), winter [December January February (DJF)] and *B*, summer [June July August (JJA)] (*Left*). (*C*) and (*D*) Differences in simulated mean annual temperature with the $4 \times CO_2$ Cretaceous (Eocene minus Cretaceous). The Eocene climate is generally cooler during the wintertime and warmer in the summer throughout the mid- to high-latitudes in both hemispheres. Only temperature differences exceeding the 95% confidence limits are displayed in (*C*) and (*D*).

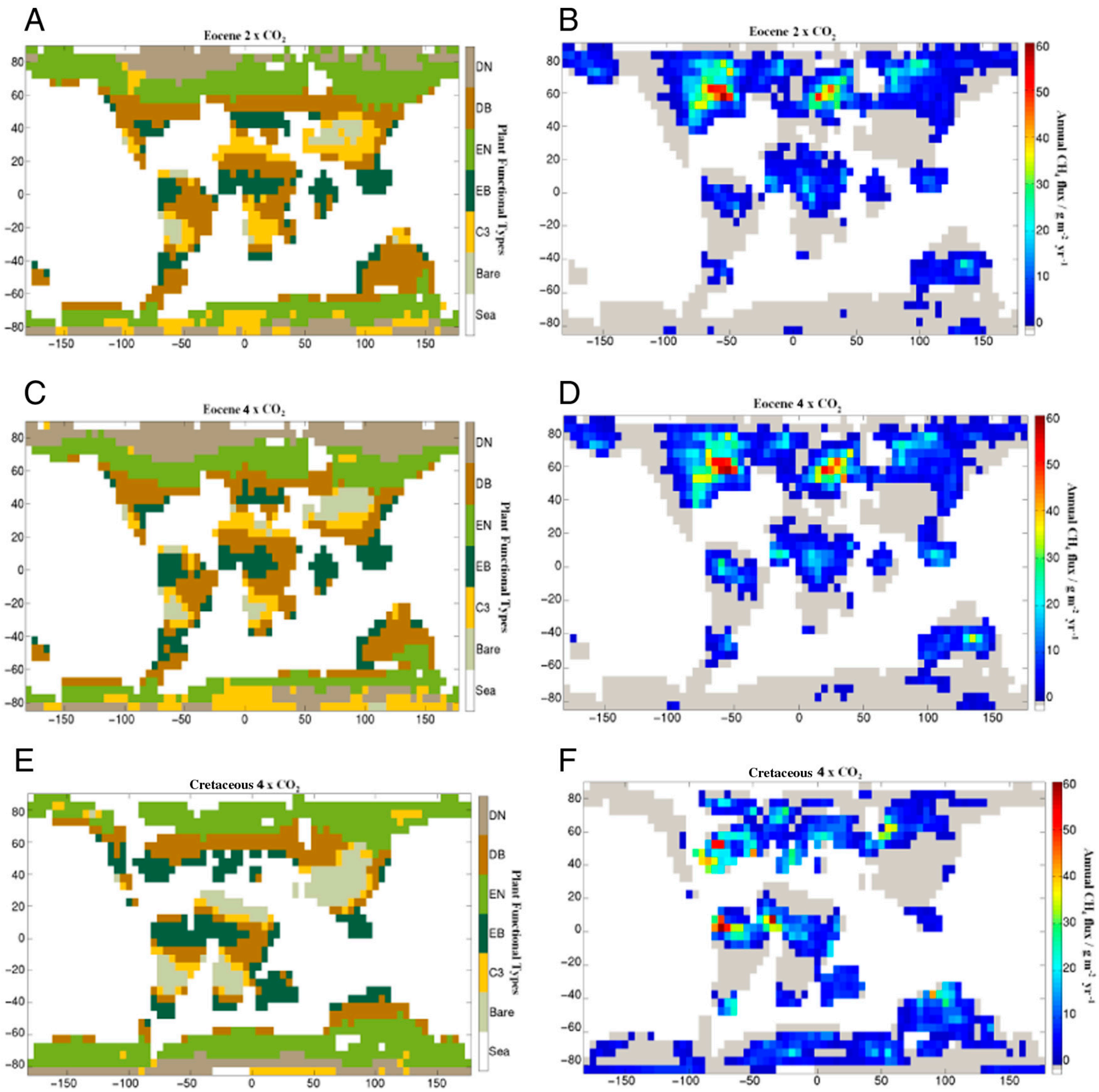

Fig. S2. Simulated global distribution of plant functional types (PFTs) (*A*, *C* and *E*) and wetland annual CH_4 fluxes (*B*, *D* and *F*) for the $2 \times CO_2$ and $4 \times CO_2$ Eocene climates and the $4 \times CO_2$ Cretaceous climate. PFTs in (*A*, *C* and *E*): DN, deciduous needle-leaved forest; DB, deciduous broad-leaved forest; EN, evergreen needle-leaved forests; EB, evergreen broad-leaved forest; C_3, shrubs with the C_3 photosynthetic pathway; bare, bare-ground. Annual wetland CH_4 emissions in (*B*, *D* and *F*) mapped after correction for subgrid scale orographic variance. See Table S1 for areas and methane fluxes.

Table S1. Simulated sources of biogenic trace gas emissions during the early Eocene and late Cretaceous. Fluxes for the PI given in (20)

Early Eocene (55 Ma)	$2 \times CO_2$ climate				$4 \times CO_2$ climate			
	NH (90-30 °N)	Tropics (30 °N-30 °S)	SH (30-90 °S)	Total	NH (90-30 °N)	Tropics (30 °N-30 °S)	SH (30-90 °S)	Total
Annual wetland area (10^6 km^2)	17.4	12.9	4.2	34.2	17.4	12.8	3.8	34.0
Wetland CH_4	414.7	301.0	80.0	795.7	649.4	349.1	144.1	1142.6
CH_4 from biomass burning	5.3	12.6	2.0	19.9	8.6	15.8	3.0	27.4
CH_4 from oceans (+ termites)	3.4 (9.5)	4.0 (14.5)	5.6 (3.0)	13.0 (27.0)	3.4 (11.3)	4.0 (13.0)	5.6 (2.7)	13.0 (27.0)
Total CH_4 (Tg CH_4 yr^{-1})				**855.6**				**1210.0**
Isoprene (Tg C yr^{-1})	98.1	1107.6	30.8	1236.5	187.5	1426.0	47.3	1660.8
Monoterpene (Tg C yr^{-1})	66.4	86.8	16.2	169.4	117.7	111.5	22.3	251.5
Other reactive VOCs (Tg C yr^{-1})	194.6	220.0	71.9	486.5	252.8	222.8	87.0	562.6
Soil NO_x(Tg N yr^{-1})	0.61	2.7	0.4	3.7	0.49	3.0	0.36	3.9
NO_x from burning (Tg N yr^{-1})	2.7	6.5	1.0	10.2	3.3	6.2	1.0	10.5
NO_x from lightning	2.1	6.5	0.2	8.8	2.5	7.7	0.2	10.4
Soil N_2O(Tg N yr^{-1})	3.7	8.4	1.5	13.6	3.1	7.5	1.9	11.5
N_2O from burning (Tg N yr^{-1})	0.4	0.85	0.15	1.39	0.7	1.1	0.2	2.0
CO from burning (Tg C yr^{-1})	92.5	233.7	35.3	361.5	152.3	288	51.8	492.1

Late Cretaceous (90 Ma)	$4 \times CO_2$ climate			
	NH (90-30 °N)	Tropics (30 °N-30 °S)	SH (30-90 °S)	Total
Annual wetland area (10^6 km^2)	10.5	8.4	7.3	26.2
Wetland CH_4	372.7	247.2	237.1	857.0
CH_4 from biomass burning	3.7	5.3	2.8	11.8
CH_4 from oceans (+ termites)	4.3 (7.8)	4.0 (13.5)	4.7 (5.7)	13.0 (27.0)
Total CH_4 (Tg CH_4 yr^{-1})				**908.8**
Isoprene (Tg C yr^{-1})	178.7	936.5	85.6	1200.8
Monoterpene (Tg C yr^{-1})	52.0	90.4	38.6	181.0
Other reactive VOCs (Tg C yr^{-1})	174.0	126.2	128.6	428.8
Soil NO_x (Tg N yr^{-1})	0.63	2.21	0.7	3.5
NO_x from burning (Tg N yr^{-1})	1.9	2.7	1.4	6.0
NO_x from lightning	1.6	4.9	0.2	6.7
Soil N_2O (Tg N yr^{-1})	5.4	7.5	2.4	15.3
N_2O from burning (Tg N yr^{-1})	0.27	0.35	0.2	0.82
CO from burning (Tg C yr^{-1})	67.0	97.3	50.5	214.8

Table S2. Global tropospheric methane budgets and methane lifetimes

	Methane budget terms					
Simulation	Burden (Tg)	$CH_4 + OH$ loss ($Tg\,yr^{-1}$)	Stratospheric loss ($Tg\,yr^{-1}$)	Dry deposition ($Tg\,yr^{-1}$)	Total losses	Lifetime (years)
Preindustrial (PI, 0 Ma)						
$1 \times CO_2$ (280 ppm)	1,800	221	7	25	253	7.1
Early Eocene (55 Ma)						
$2 \times CO_2$ (560 ppm)	6,624	693	13	132	838	7.9
$2 \times CO_2$ (PI isoprene flux)	6,051	713	12	122	847	7.2
$4 \times CO_2$ (1,120 ppm)	8,552	906	14	171	1,091	7.8
$4 \times CO_2$ (PI isoprene flux)	7,875	933	13	158	1,104	7.1
Late Cretaceous (90 Ma)						
$4 \times CO_2$ (1,120 ppm)	8,190	774	13	92	879	9.3

Lifetime calculated as the methane burden divided by the sum of all methane loss fluxes.

Table S3. Global hydroxyl radical (OH) budgets

	Simulation					
OH Sources (Tmol/yr)	$2 \times CO_2$ Eocene	$2 \times CO_2$ Eocene (PI isop.)	$4 \times CO_2$ Eocene	$4 \times CO_2$ Eocene (PI isop.)	$4 \times CO_2$ Cretaceous	Preindustrial
$H_2O + O_1D \rightarrow 2OH$	112.78	104.98	143.74	126.39	119.07	59.26
$HO_2 + NO \rightarrow NO_2 + OH$	71.29	58.25	90.71	68.73	74.85	37.21
$H_2O_2 + hv \rightarrow 2OH$	34.64	25.63	49.49	28.24	39.83	14.35
$HO_2 + O_3 \rightarrow OH + 2O_2$	25.55	19.02	33.43	22.97	28.79	12.04
$CH_3OOH + hv \rightarrow HCHO + HO_2 + OH$	7.19	6.31	10.28	8.82	8.72	2.12
$ISOPOOH + hv \rightarrow MVK + HCHO + HO_2$	1.60	0.56	2.05	0.53	1.53	0.84
$MVKOOH + hv \rightarrow MGLYOX + HCHO + HO_2$	1.22	0.33	1.54	0.3	1.15	0.67
$O_3 + C_5H_8 \rightarrow MVK + .22HCHO + .78CO +$	1.47	0.31	2.05	0.29	1.50	0.58
$O_3 + MVK \rightarrow MGLYOX + .24HCHO + .76CO$	1.42	0.35	2.03	0.35	1.51	0.55
Other terms	0.20	0.16	0.29	0.20	0.26	0.11
Total OH production:	257.36	215.90	335.61	256.82	277.21	127.73
OH Sinks (Tmol/yr)						
$CO + OH \rightarrow CO_2 + HO_2$	105.73	77.18	140.02	92.96	117.26	50.72
$CH_4 + OH \rightarrow CH_3O_2 + H_2O$	43.34	44.54	56.65	58.37	48.39	13.84
$HCHO + OH \rightarrow HO_2 + CO$	20.51	21.10	26.96	26.07	21.28	9.56
$HO_2 + OH \rightarrow H_2O + O_2$	11.57	11.51	13.53	12.75	11.07	9.51
$C_5H_8 + OH \rightarrow RO_2IP1$	14.68	7.00	19.38	7.03	14.00	8.21
$OH + O_3 \rightarrow HO_2 + O_2$	8.54	8.69	9.48	9.31	8.13	7.58
$OH + MVK \rightarrow RO_2IP2$	13.19	6.24	17.52	6.34	12.55	7.15
$H_2O_2 + OH \rightarrow HO_2$	11.04	12.22	15.19	10.61	11.81	5.74
$CH_3OOH + OH \rightarrow CH_3O_2 + H_2O$	14.24	14.25	19.02	18.52	15.46	5.45
$H_2 + OH \rightarrow HO_2$	5.58	4.37	6.97	4.92	7.98	4.1
$MGLYOX + OH \rightarrow CH_3COO_2 + CO$	2.37	1.78	3.35	2.00	2.42	1.29
$NO_2 + OH \rightarrow HNO_3$	1.49	1.61	1.78	1.88	1.59	0.93
$CH_3OH + OH \rightarrow HCHO + HO_2$	1.72	1.98	2.17	2.61	1.88	0.55
Other terms	3.36	3.35	3.59	3.45	3.39	3.10
Total OH loss:	257.36	215.82	335.61	256.82	277.21	127.73
OH Burden (Mmol)	11.93	13.63	12.16	13.75	10.49	14.31
OH lifetime (s)	1.44	1.96	1.13	1.67	1.18	3.48

Table S4. Tropospheric ozone budget terms (P, chemical production; L, chemical loss; D, dry deposition; and S, stratospheric input—inferred as the residual of the other terms; all in $Tg(O_3)\ yr^{-1}$), burden (B, $Tg(O_3)$), and lifetime (τ, days), for the various simulations

Simulation	P	L	D	S	B	τ
Preindustrial (PI, 0 Ma)						
$1 \times CO_2$ (280 ppm)	2,574	2,606	436	468	224	26.8
Early Eocene (55 Ma)						
$2 \times CO_2$ (560 ppm)	5,036	4,920	707	591	255	16.6
$2 \times CO_2$ (PI isoprene flux)	4,173	4,065	647	538	228	17.6
$4 \times CO_2$ (1,120 ppm)	6,437	6,307	772	642	270	13.9
$4 \times CO_2$ (PI isoprene flux)	4,955	4,817	694	557	238	15.7
Late Cretaceous (90 Ma)						
$4 \times CO_2$ (1,120 ppm)	5,259	5,230	764	735	263	16.0
Present day (year 2000) for reference						
$1.3 \times CO_2$ (370 ppm)	4,974 ± 223	4,577 ± 291	953 ± 154	556 ± 154	336 ± 27	22.2 ± 2.2

Present-day estimates from a recent multimodel intercomparison (31) are also given for comparison.

Table S5.

Simulation	Radiative forcings								
	FCO_2	FCH_4	$FeCH_4$	FN_2O	ΣF $(CH_4 + N_2O)$	$FCO_2/\Sigma F$	Sc (%)	FSc	$FGHGs_{adj}$
Modern (0 Ma)									
A.D. 1880–2000	1.5	0.60	0.85	0.16	1.01	0.67	1.0	0.0	2.8
Early Eocene (55 Ma)									
$2 \times CO_2$ (560 ppm)	3.5	0.95	1.33	0.34	1.68	0.48	0.995	−1.01	4.2
$2 \times CO_2$ (PI isoprene flux)	3.5	0.88	1.23	0.34	1.58	0.45	0.995	−1.01	4.1
$4 \times CO_2$ (1,120 ppm)	6.3	1.28	1.80	0.51	2.32	0.37	0.995	−1.01	7.6
$4 \times CO_2$ (PI isoprene flux)	6.3	1.19	1.67	0.51	2.18	0.35	0.995	−1.01	7.5
Late-Cretaceous (90 Ma)									
$4 \times CO_2$ (1,120 ppm)	6.3	1.22	1.73	0.45	2.18	0.35	0.992	−1.82	6.7

Forcings for CH_4 and N_2O calculated from the analytic expressions describing radiative transfer calculations (1), with preindustrial CO_2, methane and nitrous oxide concentrations of 280 ppm, 651 ppb and 260 ppb respectively. Fe is the effective forcing by methane accounting for indirect forcing arising from increases in stratospheric water vapor and ozone (40%) (2). Solar radiation has gradually increased with the evolution of the Sun. This column provides estimated change in solar output (Sc) in the past as a percentage of the present-day value (3). Calculated change in radiative forcing from solar output (3). Column $FGHGs_{adj}$ gives total radiative forcing by all greenhouse gases after correction for change in FSc.

1 Hansen J, et al. (2000) Global warming in the twenty first century: an alternative scenario. *Proc Natl Acad Sci USA* 97:9875–9880.
2 Hansen J, et al. (2007) Climate change and trace gases. *Philos T R Soc S-A* 365:1925–1954.
3 Berner RA (2004) *The Phanerozoic Carbon Cycle* (Oxford University Press, Oxford).